Analysis of coupled energy and helicity spectra in stratified turbulence: Theory and balloon measurements

Niklas Dusch [*]
Meteorological Institute, Universität Hamburg, Hamburg 20146, Germany and Universität Potsdam, Potsdam 14476, Germany

Victor Avsarkisov [†]
Meteorological Institute, Universität Hamburg, Hamburg 20146, Germany

Michael Gerding and Claudia Stolle
Leibniz Institute of Atmospheric Physics, Kühlungsborn 18225, Germany

Jens Faber [‡]
Leibniz Institute for Baltic Sea Research, Rostock 18119, Germany

(Received 22 March 2023; accepted 2 February 2024; published 6 March 2024)

In this study, we propose a new theoretical approach to describe the spectra of kinetic energy and helicity under the influence of stratification. We introduce a scaling parameter m and perform the scaling analysis, which allows us to consider the effect of stratification on the spectra. It becomes possible to categorize the spectral properties of energy, helicity, and dual cascades in stratified turbulent flows based on the energy- and helicity-dominated cascade scenarios. New scaling laws for dual cascade scenarios in flows with a strong stratification are formulated as well. The comparison of the theoretical results against atmospheric balloon-borne observations reveals that slopes of the energy cascades are typically steeper than the helicity ones. This is an indication of the energy-dominated cascade behavior at considered scale ranges and altitude segments.

DOI: 10.1103/PhysRevFluids.9.033801

I. INTRODUCTION

Sheared turbulent flows are ubiquitous in nature, applications of fluid mechanics, and environmental flows. Moreover, under the influence of gravity, these flows exhibit the effect of stratification. Thus, the comprehensive description of stratified and sheared flow is crucial for understanding the main aspects of the physics shaping our environment.

The multiscale nature of turbulent flows enhances their complexity. Turbulence develops distinctive nonlinear dynamics with complex, chaotic, and intermittent behavior. The Navier-Stokes equations, which describe the stratified turbulent flows, are analytically nonresolvable and require simplification for further investigation. One of the most useful tools to explore stratified turbulence is the energy spectrum, which is based on the well-known turbulence property of the energy cascade

[*]Previously at Physics Department, University of Rostock, Rostock, Germany and Leibniz Institute of Atmospheric Physics Kühlungsborn, Germany.
[†]Previously at Leibniz Institute of Atmospheric Physics, Kühlungsborn, Germany; victor.avsarkisov@uni-hamburg.de
[‡]Previously published under the name Jens Söder.

through the scales within the flow. This method describes how conserved energy is spectrally distributed in the wave-number space.

In flows with a direct cascade, the energy is transferred from large to small length scale structures. This mechanism is a so-called Richardson's energy cascade [1]. For homogeneous isotropic turbulence (HIT) flows, this direct cascade process results in $E(k) \sim k^{-\frac{5}{3}}$ [2–4] spectral behavior, whereas, under the influence of stratification, the direct cascade prediction exhibits a k^{-3} spectrum [5–7]. The physical mechanism that builds the spectrum of stratified turbulence is still not sufficiently understood, and the latter spectral prediction requires experimental and numerical confirmation [3,6,8]. Thus, it is tempting to ask whether the spectral representation of the kinetic energy can be complemented by an additional conserved parameter that may provide further insights into the dynamics of stratified turbulence. In the present study, we evaluate if the kinetic helicity can serve as such quantity.

As first discovered in the 1960s by Moreau [9] and Moffatt [10], kinetic helicity is a conserved quantity under certain conditions, and it became a powerful tool for fluid mechanical descriptions. In another fundamental study by Moffatt and Tsinober [11], the significance of kinetic helicity for turbulent flows is investigated by describing the behavior and the evolution of vortices affected and shaped by it. Brissaud *et al.* [12] made essential considerations on how helical dynamics can contribute to the description of turbulent flows and analyzed their dynamical properties. The concept of treating cascades of energy and helicity in a similar way was introduced in this context. Numerous studies have examined the properties of kinetic helicity in rotating and stratified turbulent flows [13–18]. Analogously to the kinetic energy, one key aspect of interest in these studies was the analysis of the spectrum of kinetic helicity in the wave-number space to describe the spectral behavior of kinetic helicity throughout the scales as proposed in Brissaud *et al.* [12].

In atmospheric physics, a parametrization of the helical turbulence was proposed by Levina [19] to analyze the influence of small-scale helical turbulence on tropical cyclones. Adding an extra forcing term into the equation of thermal convection in the Boussinesq approximation allowed authors to model some typical features of atmospheric vortices, such as the generation of intense azimuthal circulation and intensification of vertical circulation. An extensive analysis of the role of helicity in the Ekman boundary layer was performed in the last 30 years [13,20–26] as well. Yet, there is still no comprehensive theory of kinetic helicity and its spectral properties in stratified turbulence. Furthermore, the question arises whether the kinetic helicity could serve as a tool to determine and explain characteristic dynamics in the presence of stratification, such as turbulent layered pancakelike vortical structures (LPS) and internal gravity waves (GWs) in the layered anisotropic stratified turbulence (LAST) regime.

In the second section, we formulate the scaling approach to describe general forms for the spectra of kinetic energy and kinetic helicity in stratified turbulent flows and present the obtained theoretical results. Our approach employs the idea of distinct helicity transfer timescale in dual cascading systems, introduced for three-dimensional HIT by Kurien *et al.* [27] and applies it to vertically anisotropic stratified turbulence. The analysis of experimental balloon data, including the computation of kinetic energy and kinetic helicity spectra in different flow conditions, is performed in the third section. In the final section, we discuss the results and summarize the main conclusions.

II. SPECTRA OF KINETIC ENERGY AND KINETIC HELICITY FOR STRATIFIED TURBULENT FLOWS

In the following, we consider only flows that obey the stationary Boussinesq equations without rotation

$$(\vec{u} \cdot \nabla)\vec{u} = -\frac{\nabla p}{\bar{\rho}} + \frac{\rho'}{\bar{\rho}}\vec{g} + \nu \Delta \vec{u}. \tag{1}$$

Here $\vec{u}$ is the three-dimensional velocity, p is the pressure, $\bar{\rho}$ the mean density, ρ' is the density fluctuation, and ν is the kinematic viscosity of the flow. The gravity force acts in vertical z direction, hence $\vec{g} = -g\vec{e}_z$. Here $\vec{e}_z$ denotes the unit vector in the vertical direction and g is the gravitational acceleration. We omit any further external force; thus, the anisotropy of the flow solely occurs as a buoyancy force effect.

The magnitude of stratification is characterized by the dimensionless parameters of the Froude number

$$\mathrm{Fr} = \frac{U}{Nl}, \tag{2}$$

depicting the ratio of inertial forces to the buoyancy force, and the Richardson number

$$\mathrm{Ri} = \frac{N^2}{(\partial u/\partial z)^2 + (\partial v/\partial z)^2}, \tag{3}$$

relating buoyancy and vertical velocity shear. The relationship between the nondimensional parameters Ri and Fr in shear-dominated turbulence is expressed as $\mathrm{Ri} = \mathrm{Fr}^{-2}$, but this relationship does not hold in more general cases. Here, l and U are the characteristic length and velocity scales, respectively, and $\partial u/\partial z$ and $\partial v/\partial z$ are the vertical gradients of the horizontal velocity components. The Brunt-Väisälä frequency N is defined as

$$N = \sqrt{-\frac{g}{\bar{\rho}}\frac{\mathrm{d}\rho_0}{\mathrm{d}z}}. \tag{4}$$

The kinetic energy, helicity, and enstrophy contained in the volume $\mathcal{V}$ are defined as

$$E_v = \int_{\mathcal{V}} \vec{u}\cdot\vec{u}\,\mathrm{d}^3 r, \tag{5}$$

$$H_v = \int_{\mathcal{V}} \vec{u}\cdot\vec{\omega}\mathrm{d}^3 r, \tag{6}$$

$$Z_v = \int_{\mathcal{V}} \vec{\omega}\cdot\vec{\omega}\,\mathrm{d}^3 r \tag{7}$$

with $\vec{\omega} = \nabla \times \vec{u}$ denoting the flow vorticity. The so-called relative helicity can be defined as

$$\sigma = \frac{H_v}{\sqrt{E_v Z_v}}. \tag{8}$$

From the Cauchy-Schwarz inequality, it follows that $-1 \leqslant \sigma \leqslant 1$. In the case of zero relative helicity $\sigma = 0$, the total amount of the kinetic helicity is zero too. The maximum relative helicity $\sigma = 1$ corresponds to a case with maximal kinetic helicity. Unlike the energy (E_v), kinetic helicity (H_v), or kinetic enstrophy (Z_v), σ is independent of the flow volume. Considering, for instance, a system with constant velocity, the kinetic energy will be proportional to the integration volume. Similarly, a flow of high kinetic helicity may be either strongly helical or have a large volume. Hence, the three quantities: E_v, H_v, and Z_v are so-called extensive quantities. The relative helicity, in contrast, is independent of the system volume, which makes it a powerful measure to compare different flows.

A. Approach

In the present study, it is assumed that the spectra of kinetic energy E and kinetic helicity H are functions of a wave number k in the form of power laws [18,28]

$$E(k) \sim k^{-\kappa_E}, \tag{9}$$

$$H(k) \sim k^{-\kappa_H}. \tag{10}$$

Here κ_E and κ_H are the corresponding slope constants, and the wave number k represents either the total wave number $k = |\vec{k}|$ in the HIT case or the vertical wave number k_z in the LAST case.

According to Brissaud *et al.* [12], it is possible to describe three different cascade scenarios in three-dimensional HIT.

(i) Pure energy downward cascade with no helicity cascade

$$\varepsilon_E \equiv \varepsilon_E(k) \sim \frac{kE(k)}{\tau_{tr}(k)} = \text{const.}, \tag{11}$$

$$\varepsilon_H = 0. \tag{12}$$

This process is characterized by a constant rate of transfer of kinetic energy ε_E through the scales.

(ii) Joint energy and helicity downward cascade

$$\varepsilon_E \equiv \varepsilon_E(k) \sim \frac{kE(k)}{\tau_{tr}(k)} = \text{const.}, \tag{13}$$

$$\varepsilon_H \equiv \varepsilon_H(k) \sim \frac{kH(k)}{\tau_{tr}(k)} = \text{const.}, \tag{14}$$

a simultaneous dual cascade of both quantities through the scales.

(iii) Finally they did not exclude the theoretical possibility of pure helicity cascade with no energy cascade

$$\varepsilon_E = 0, \tag{15}$$

$$\varepsilon_H \equiv \varepsilon_H(k) \sim \frac{kH(k)}{\tau_{tr}(k)} = \text{const.}, \tag{16}$$

indicating the complexity of the system with these cascading properties and not specifying the direction of the helicity cascade.

Perhaps the main limitation for authors of Brissaud *et al.* [12] in characterizing these different cascading scenarios was an assumption of the energy-dominated (energy-driven) transfer time τ_{tr} (the distortion time therein and in Kraichnan [29]) for energy and helicity transfer

$$\tau_{tr}(k) \sim \left(\int_0^k p^2 E(p) dp\right)^{-1/2} \sim [E(k)k^3]^{-1/2} \sim \tau_E. \tag{17}$$

They proposed the transfer time τ_{tr} as a measure of the characteristic timescale of the energy cascade assuming that in all three cases cascades are governed by τ_{tr} defined as (17).

In their seminal paper Kurien *et al.* [27] proposed the helicity-dominated (helicity-driven) joint cascading scenario [case (ii)] with the characteristic timescale

$$\tau_{tr}(k) \sim \left(\int_0^k p^2 E(p) dp\right)^{-1/2} \sim \left(\frac{1}{2}|H(k)|k^2\right)^{-1/2} \sim \tau_H \tag{18}$$

for both kinetic energy and helicity cascades. The result of this consideration is a shallow spectrum with $k^{-4/3}$ scaling in both energy and helicity. Authors also suggested that $k^{-5/3}$ scaling must be observed at large scales within the inertial subrange, while the former $k^{-4/3}$ scaling characterizes small scales of the inertial subrange.

In the present study, we consider the competing cases of dynamics governed by kinetic energy according to (17) or kinetic helicity according to (18) that have been discussed in the context of HIT. These timescales are applied to stratified, hence characteristically anisotropic flows. In the following, we denote them as the energy-dominated or the helicity-dominated cases. However, consideration of the stratification effect requires an additional assumption.

The phenomenology of weak turbulence theory [30,31] allows us to decompose the flow into fast and slow velocity manifolds. To estimate the effect of stratification on the transfer timescale, we consider that the temporal scale of the buoyancy force effects is proportional to the Brunt-Väisälä frequency N, namely $\tau_{\mathrm{GW}} = N^{-1}$. In the atmospheric flows, this assumption is valid for the small-scale (typically hundreds of meters horizontal scales down to the Ozmidov scale) motions, namely, gravity waves.

Thus, under the influence of stratification, relations between τ_{tr} and τ_E, τ_H [see Eq. (17), (18)] require the following modification:

$$\tau_{tr} = \tau_E \frac{\tau_E}{\tau_{\mathrm{GW}}} \quad \text{or} \quad \tau_{tr} = \tau_H \frac{\tau_H}{\tau_{\mathrm{GW}}}, \tag{19}$$

where τ_{GW} denotes the period of small-scale gravity waves. A similar approach is used in Ref. [28] for the case with rotating turbulence.

The ratio $\tau_E \tau_{\mathrm{GW}}^{-1}$ can be represented as the multiplicative inverse of the Froude number Fr. This number is below unity in stratified flows and decreases as stratification increases. Thus, the transfer time increases in the presence of stratification and indicates the slowdown of the energy cascade. In other words, the dynamics related to stratification inhibit the transfer process.

We now introduce an additional generalization to the transfer timescale definitions, namely

$$\tau_{\mathrm{tr}} = \tau_E \delta_E^m = \tau_E^{1+m} N^m, \tag{20}$$

$$\tau_{\mathrm{tr}} = \tau_H \delta_H^m = \tau_H^{1+m} N^m, \tag{21}$$

with

$$\delta_E = \frac{\tau_E}{\tau_{\mathrm{GW}}}, \tag{22}$$

$$\delta_H = \frac{\tau_H}{\tau_{\mathrm{GW}}}, \tag{23}$$

for the energy-dominated (20), (22) and helicity-dominated (21), (23) cases, respectively. The introduction of m as a nondimensional parameter enables quantification of the stratification effect. For $m = 0$, stratification has no direct impact on the cascading process, while for increasing m, δ^m becomes large and increases the transfer time. Moreover, it enables us to extend the assumption concerning the form of the spectra analogously to Ref. [28]

$$E(k) \sim \varepsilon_E^{a_E} \varepsilon_H^{b_E} N^{c_E} k^{-\kappa_E}, \tag{24}$$

$$H(k) \sim \varepsilon_E^{a_H} \varepsilon_H^{b_H} N^{c_H} k^{-\kappa_H}. \tag{25}$$

In the following section, we analyze all possible cascade scenarios (energy cascade, helicity cascade, and joint cascade), as proposed in Brissaud *et al.* [12], for two competing cases of either kinetic energy domination or helicity domination. Moreover, variation of m enables us to consider different impacts of stratification on cascades.

In some cases, the proposed method does not suffice to make a statement on the spectra of kinetic energy and kinetic helicity. Nevertheless, for these cases, it is helpful to consider that the rate of transfer of kinetic helicity should go to zero for large wave numbers in energy-dominated cases [12]

$$\frac{kH(k)}{\tau_{tr}(k)} \to 0 \quad \text{for} \quad k \to \infty. \tag{26}$$

Analogous condition should hold for the kinetic energy cascade in helicity-dominated cases

$$\frac{kE(k)}{\tau_{tr}(k)} \to 0 \quad \text{for} \quad k \to \infty. \tag{27}$$

B. Energy-dominated distortion ($\tau_{\mathrm{tr}} = \tau_E \delta_E^m$)

1. Energy cascade ($\varepsilon_E = const.$)

In case of energy-dominated scenario, for the cascade of energy with constant energy flux (11) and the transfer time (20) we obtain

$$E(k) \sim \varepsilon_E \frac{1}{k} \tau_E^{1+m} N^m \sim \varepsilon_E \frac{1}{k} [k^3 E(k)]^{-\frac{1+m}{2}} N^m \sim \varepsilon_E N^m k^{-\frac{5+3m}{2}} E(k)^{-\frac{1+m}{2}}, \tag{28}$$

which provides

$$E(k) \sim \varepsilon_E^{\frac{2}{3+m}} N^{\frac{2m}{3+m}} k^{-\frac{5+3m}{3+m}} \tag{29}$$

with

$$\kappa_E = \frac{5+3m}{3+m}. \tag{30}$$

For case without stratification ($m = 0$) one retrieves Kolmogorov's $k^{-5/3}$ spectrum [2]

$$E(k) \sim \varepsilon_E^{2/3} k^{-5/3}. \tag{31}$$

However, if $m \to \infty$, we obtain the spectrum for the buoyancy subrange in stratified turbulence of the form [5,32–34].

$$E(k) \sim N^2 k^{-3}. \tag{32}$$

For the kinetic helicity spectrum, (26) provides

$$\begin{aligned} \varepsilon_H \sim \frac{kH}{\tau_{\mathrm{tr}}} \sim k^{1-\kappa_H} [k^3 k^{-\kappa_E}]^{\frac{m+1}{2}} \to 0\,(k \to \infty) \\ \Rightarrow 0 > -\kappa_H + \frac{5}{2} + \frac{3}{2} m - \kappa_E \frac{1+m}{2} \end{aligned} \tag{33}$$

and thus

$$\kappa_H > \frac{5+3m}{3+m}. \tag{34}$$

Hence, dimensional analysis implies that the spectrum of kinetic helicity should be steeper than that of kinetic energy in the energy-dominated regime.

2. Helicity cascade ($\varepsilon_H = const.$)

For a helicity cascade, we can rearrange expression (16) to obtain

$$H(k) \sim \varepsilon_H k^{-\frac{5+3m}{2}} N^m E^{-\frac{1+m}{2}}. \tag{35}$$

With (9) and (10), this is equivalent to

$$\kappa_H = \frac{5+3m}{2} - \frac{1+m}{2} \kappa_E \Leftrightarrow \kappa_E = \frac{5+3m}{1+m} - \frac{2}{1+m} \kappa_H. \tag{36}$$

One thus obtains a condition linking the spectrum of kinetic helicity to the spectrum of kinetic energy. Moreover, with (27), one obtains

$$\kappa_E > \frac{5+3m}{3+m}, \tag{37}$$

which according to (36) is equivalent to

$$\kappa_H < \frac{5+3m}{3+m}. \tag{38}$$

Hence, there are no explicit expressions for κ_E and κ_H in this cascade scenario, but a condition that links constants and respective limits. Although the exponents have no fixed values, the corresponding spectral slope constants for kinetic energy and helicity are coupled. It follows from the derived inequalities that the spectrum of kinetic energy has to be steeper than the one of kinetic helicity.

3. Dual cascade (ε_E = const., ε_H = const.)

For the dual cascade case, both transfer rates (ϵ_E and ϵ_H) are constant. Thus, the kinetic energy spectrum is derived in the same way as for the energy cascade scenario in Sec. II B 1 [see (29) with (30)].

The expression (36) for κ_H is the same for both the dual cascade and helicity cascade, as they both depend on κ_E. Combining this expression with (30) results in

$$\kappa_H = \frac{5+3m}{3+m}. \tag{39}$$

Thus, both spectra have the same dependence on k. Using (35) with (29) one obtains

$$H(k) \sim \varepsilon_E^{-\frac{1+m}{3+m}} \varepsilon_H N^{\frac{2m}{3+m}} k^{-\frac{5+3m}{3+m}}. \tag{40}$$

For $m = 0$, the spectra found for the energy and the helicity correspond to the dual cascade scenario from Brissaud *et al.* [12]

$$E(k) \sim \varepsilon_E^{2/3} k^{-5/3}, \tag{41}$$

$$H(k) \sim \varepsilon_H \varepsilon_E^{-1/3} k^{-5/3}. \tag{42}$$

By setting $m = 2$ we recover the Bolgiano-Obukhov scaling,

$$E(k) \sim \varepsilon_E^{2/5} N^{4/5} k^{-11/5}, \tag{43}$$

$$H(k) \sim \varepsilon_H \varepsilon_E^{-3/5} N^{4/5} k^{-11/5}. \tag{44}$$

Finally, for $m \to \infty$ we obtain the spectral relation for the energy-dominated dual cascade scenario with strong stratification.

$$E(k) \sim N^2 k^{-3}, \tag{45}$$

$$H(k) \sim \varepsilon_H \varepsilon_E^{-1} N^2 k^{-3}. \tag{46}$$

This dual cascade scenario has not yet been presented in the literature and requires further verification.

C. Helicity-dominated distortion ($\tau_{\mathrm{tr}} = \tau_H \delta_H^m$)

1. Energy cascade (ε_E = const.)

Analogously to the energy-dominated energy cascade from Sec. II B 1, the helicity-dominated energy cascade is characterized by (11). However, the transition time in the present case is based on the helicity-dominated distortion time according to (21).

Using the definition of τ_H, one obtains

$$E(k) \sim \varepsilon_E k^{-2-m} H(k)^{-\kappa_H \frac{1+m}{2}} N^m. \tag{47}$$

Assuming $E(k) \sim k^{-\kappa_E}$ and $H(k) \sim k^{-\kappa_H}$, we obtain the coupling property between κ_E and κ_H.

$$\kappa_E = 2 + m - \frac{1+m}{2}\kappa_H \tag{48}$$

$$\Leftrightarrow \kappa_H = \frac{4+2m}{1+m} - \frac{2}{1+m}\kappa_E. \tag{49}$$

This property allows us to infer the value of m (or the magnitude of stratification) if the coupled slope constants are known.

Moreover, using (26), the conditions

$$\kappa_H > \frac{4+2m}{3+m}, \tag{50}$$

$$\kappa_E < \frac{4+2m}{3+m} \tag{51}$$

are obtained. Hence, the exponents of both spectra are limited to some values. It also follows that the kinetic helicity spectrum is always steeper than the kinetic energy one in the helicity-dominated energy cascade scenario. This result is the opposite of the exponent conditions (37) and (38) for an energy-dominated helicity cascade (see Sec. II B 2).

2. *Helicity cascade* ($\varepsilon_H = const.$)

For a pure helicity cascade with the constant rate of helicity transfer (16) one obtains

$$H \sim \varepsilon_H^{\frac{2}{3+m}} k^{-\frac{4+2m}{3+m}} N^{\frac{2m}{3+m}}, \tag{52}$$

$$\kappa_H = \frac{4+2m}{3+m}. \tag{53}$$

The value of the exponent of the spectrum (κ_H) is smaller than the limit for the respective value for the energy-dominated helicity cascade (38) and smaller than the corresponding values for the energy-dominated energy cascade (34) and dual cascade (39). Thus, the spectrum of kinetic helicity tends to be shallower in the helicity-dominated helicity cascade.

Moreover, (27) provides an expression for κ_E as

$$\kappa_E > \frac{4+2m}{3+m}. \tag{54}$$

This suggests that the spectrum of kinetic energy is steeper than that of kinetic helicity in a helicity-dominated scenario.

3. *Dual cascade* ($\varepsilon_E = const.$, $\varepsilon_H = const.$)

For the case of a helicity-dominated dual cascade, we again assume the constant rate of transfer of kinetic helicity (14) and obtain the helicity spectrum in the following form:

$$H \sim \varepsilon_H^{\frac{2}{3+m}} k^{-\frac{4+2m}{3+m}} N^{\frac{2m}{3+m}}, \tag{55}$$

$$\kappa_H = \frac{4+2m}{3+m}. \tag{56}$$

Since for the dual cascade, the energy transfer rate is also constant and follows (13), one obtains equation (48). With (56), the latter condition is equivalent to

$$\kappa_E = \frac{4+2m}{3+m}. \tag{57}$$

Thus, the values for the exponents of the spectra of kinetic energy and kinetic helicity are equal. The spectra of the helicity-dominated dual cascade scenario are shallower when compared to the energy-dominated ones.

Using (47) and inserting (55), one obtains

$$E(k) \sim \varepsilon_E \varepsilon_H^{-\frac{1+m}{3+m}} N^{\frac{2m}{3+m}} k^{-\frac{4+2m}{3+m}}. \tag{58}$$

TABLE I. Different cascade cases are distinguished, based on the cascading quantity (kinetic energy, kinetic helicity, or both) and the quantity determining the transfer time (τ_E for dominant kinetic energy, τ_H for dominant kinetic helicity). κ_E is the exponent for an energy spectrum of the form $E(k) \sim k^{-\kappa_E}$. Columns consider differences in the magnitude of the influence of stratification. The m column represents the general form of κ_E. The condition $m = 0$ is equivalent to the absence of an influence of stratification whereas $m \to \infty$ represents a maximum influence of stratification.

	κ_E				
	m	0	1	2	∞
Energy cascade (τ_E)	$\frac{5+3m}{3+m}$	$\frac{5}{3}$	2	$\frac{11}{5}$	3
Helicity cascade (τ_E)	$> \frac{5+3m}{3+m}$	$> \frac{5}{3}$	>2	$> \frac{11}{5}$	>3
	$\frac{5+3m}{1+m} - \frac{2}{1+m}\kappa_H$	$5 - 2\kappa_H$	$4 - \kappa_H$	$\frac{11}{3} - \frac{2}{3}\kappa_H$	
Dual cascade (τ_E)	$\frac{5+3m}{3+m}$	$\frac{5}{3}$	2	$\frac{11}{5}$	3
Energy cascade (τ_H)	$< \frac{4+2m}{3+m}$	$< \frac{4}{3}$	$< \frac{3}{2}$	$< \frac{8}{5}$	<2
	$2 + m - \frac{1+m}{2}\kappa_H$	$2 - \frac{\kappa_H}{2}$	$3 - \kappa_H$	$4 - \frac{3}{2}\kappa_H$	
Helicity cascade (τ_H)	$> \frac{4+2m}{3+m}$	$> \frac{4}{3}$	$> \frac{3}{2}$	$> \frac{8}{5}$	>2
Dual cascade (τ_H)	$\frac{4+2m}{3+m}$	$\frac{4}{3}$	$\frac{3}{2}$	$\frac{8}{5}$	2

In the absence of stratification ($m = 0$), expressions (55) and (58) reproduce the spectrum of kinetic energy from Kurien *et al.* [27]

$$E(k) \sim \varepsilon_E \varepsilon_H^{-1/3} k^{-4/3}, \tag{59}$$

$$H(k) \sim \varepsilon_H^{2/3} k^{-4/3}. \tag{60}$$

In the presence of strong vertical stratification ($m \to \infty$), new scaling laws are obtained for energy and helicity spectra.

$$E(k) \sim \varepsilon_E \varepsilon_H^{-1} N^2 k^{-2}, \tag{61}$$

$$H(k) \sim N^2 k^{-2}. \tag{62}$$

These dual cascade scaling relations, analogously to (45) and (46), have not yet been reported in the literature and require careful analysis in the future.

D. Possible spectral properties of stratified turbulence

The results of the considerations of the previous subsections are summarized in Tables I and II. We present three different cascade scenarios (pure energy, pure helicity, and dual cascade) for energy-dominated and helicity-dominated cases. All six cascade scenarios are characterized by expressions for the exponents κ_E and κ_H of the powers of the wave number k. Considering the role of stratification, both their general forms (m-dependent), examples for HIT ($m = 0$), and various stratification rates ($m = 1, 2, \to \infty$) are combined in these tables.

A first conclusion to be drawn concerns the limits for values of κ_E and κ_H. After analyzing Tables I and II, we obtain that the limits for values κ_E and κ_H increase with a higher level of stratification. This means that larger limits are observed for larger m. There is a steepening of the spectrum for both kinetic energy and helicity. As discussed in Sec. II A, the slowing down of the transfer process affects this spectral steepening.

Another significant result becomes evident from comparing energy-dominated and helicity-dominated cases for either the energy, helicity, or dual cascade scenarios. For the energy-dominated

TABLE II. Different cascade cases are distinguished, based on the cascading quantity (kinetic energy, kinetic helicity, or both) and the quantity determining the transfer time (τ_E for dominant kinetic energy, τ_H for dominant kinetic helicity). κ_H is the exponent for a helicity spectrum of the form $H(k) \sim k^{-\kappa_H}$. Columns consider differences in the magnitude of the influence of stratification. The m column represents the general form of κ_H. The condition $m = 0$ is equivalent to the absence of an influence of stratification whereas $m \to \infty$ represents a maximum influence of stratification.

	κ_H				
	m	0	1	2	∞
Energy cascade (τ_E)	$> \frac{5+3m}{3+m}$	$> \frac{5}{3}$	>2	$> \frac{11}{5}$	>3
Helicity cascade (τ_E)	$< \frac{5+3m}{3+m}$	$< \frac{5}{3}$	<2	$< \frac{11}{5}$	<3
	$\frac{5+3m}{2} - \frac{1+m}{2}\kappa_E$	$\frac{5}{2} - \frac{\kappa_E}{2}$	$4 - \kappa_E$	$\frac{11}{2} - \frac{3}{2}\kappa_E$	
Dual cascade (τ_E)	$\frac{5+3m}{3+m}$	$\frac{5}{3}$	2	$\frac{11}{5}$	3
Energy cascade (τ_H)	$> \frac{4+2m}{3+m}$	$> \frac{4}{3}$	$> \frac{3}{2}$	$> \frac{8}{5}$	>2
	$\frac{4+2m}{1+m} - \frac{2}{1+m}\kappa_E$	$4 - 2\kappa_E$	$3 - \kappa_E$	$\frac{8}{3} - \frac{2}{3}\kappa_E$	
Helicity cascade (τ_H)	$\frac{4+2m}{3+m}$	$\frac{4}{3}$	$\frac{3}{2}$	$\frac{8}{5}$	2
Dual cascade (τ_H)	$\frac{4+2m}{3+m}$	$\frac{4}{3}$	$\frac{3}{2}$	$\frac{8}{5}$	2

case, the spectra and their limits are always steeper than the corresponding spectra for helicity domination. Hence, the former appears to steepen, and the helicity domination shallows spectra.

In the present study, we examined the general scaling forms of energy and helicity cascades in dual cascading scenarios. Comparison of Eq. (29) with (40) and (55) with (58) suggests the emergence of another relevant length scale

$$l_h \sim \varepsilon_E/\varepsilon_H. \tag{63}$$

The existence of the l_h was first proposed by Moiseev and Chkhetiani [35] (see also Ref. [36]) in their seminal paper on the helical scaling of turbulence. In particular, the authors predict that the length scale l_h marks the transition of the energy spectrum from the $k^{-5/3}$ for $k > l_h^{-1}$ to $k^{-7/3}$ for $k < l_h^{-1}$ in HIT. Although the effect of stratification was considered in their work, the authors did not specify its role in the emergence of l_h. Our analysis of the general scaling forms can confirm that the relation (63) turns out to be universal for the dual cascade scenarios in such a way that the form of the spectra in the energy-dominated regime is equal to the form of the spectra in the helicity-dominated regime if $k = l_h^{-1}$. Hence, l_h marks the transition between these two regimes. Additionally, for dual cascades and irrespective of the value of m, the spectrum of kinetic helicity differs from the spectrum of energy only by a factor of $\varepsilon_H/\varepsilon_E$

$$E(k) \sim \frac{\varepsilon_E}{\varepsilon_H} H(k). \tag{64}$$

The effect of vertical stratification ($m \to \infty$) provides us with another significant insight into these dynamics. Equations (45), (46) (the energy-dominated case) and Eqs. (61), (62) (the helicity-dominated case) suggest that the vertical cascade of horizontal helicity (energy) is only possible in the presence of nonzero helicity flux ε_H (nonzero energy flux ε_E) in strongly stratified energy-dominated (helicity-dominated) case.

III. BALLOON MEASUREMENTS

To analyze the energy and helicity spectra in stratified turbulence, we investigate experimental wind data from balloon measurements. These soundings were conducted using normal radiosondes of type Vaisala RS41 SG in a flight configuration for enhanced wind resolution. This special

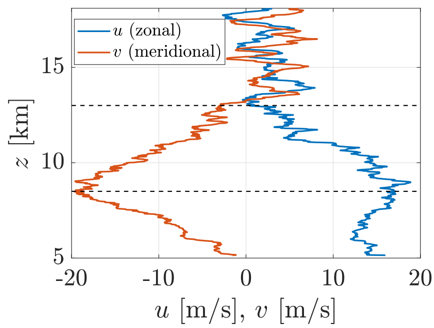

FIG. 1. Vertical profiles of zonal (blue line) and meridional (red line) components of the horizontal velocity for the 2021 dataset. Dashed lines highlight different altitude segments.

configuration is described in detail in Ref. [37]. In summary, the wind measurements are performed on the downleg path of the flight. A constant descent rate was achieved by utilizing a partly inflated balloon instead of a parachute. Radiosonde and balloon were connected by a rope of only 9 m (instead of 55 m used for upleg soundings). This short rope results in a comparatively fast pendulum motion, i.e., the spectral response maximizes at scale sizes smaller than analyzed in this study. Self-induced motions are suppressed by the choice of balloon size and descent speed, resulting in a flow around the balloon at subcritical Reynolds numbers. With the wind measurements not being disturbed by balloon or payload motions, we were able to calculate the wind speed directly from high-resolved position measurements instead of using the filtered standard data product. Practically, wind measurements were usable at scale sizes larger than 50 m. We consider two datasets, measured on 20th May 2021 (labeled as 2021) and 28th February 2022 (labeled as 2022). The data provides the two horizontal velocity components u and v measured as functions of the vertical coordinate z and time t. For the following computations, the remaining distortions from the pendulum motions of the gondola and GPS noise were removed using a low-pass filter. The velocity components represent the zonal and meridional wind, respectively. The datasets also contain profiles of pressure and temperature.

A. Measurements

Each dataset is divided into three altitude segments governed by distinct flow dynamics. The position of these segments is determined heuristically based on the wind profiles provided in Figs. 1 and 2. Thus, the vertical partition is done at heights where the velocity profiles significantly alter

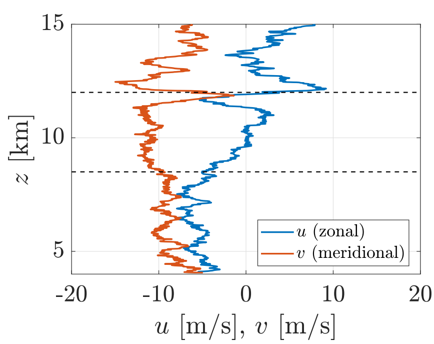

FIG. 2. Vertical profiles of zonal (blue line) and meridional (red line) components of the horizontal velocity for the 2022 dataset. Dashed lines highlight different altitude segments.

their behavior and are highlighted with dashed lines. The 2021 dataset starts at 5147 m above the ground and reaches up to 18073 m altitude, while the 2022 dataset covers the range from 4067 m up to 14977 m altitude.

Characteristic quantities provided by the measurement data are used to compute the kinetic energy, helicity, and enstrophy inside the altitude segments, defined as

$$E_{\mathcal{S}} = \int_{\mathcal{S}} (u^2 + v^2)\, \mathrm{d}z, \tag{65}$$

$$H_{\mathcal{S}} = \int_{\mathcal{S}} (-u\, \partial_z v + v\, \partial_z u)\, \mathrm{d}z, \tag{66}$$

$$Z_{\mathcal{S}} = \int_{\mathcal{S}} \left[(\partial_z v)^2 + (\partial_z u)^2\right] \mathrm{d}z, \tag{67}$$

where $\mathcal{S}$ is the altitude segment. These definitions support the properties of stratified flows [38], i.e., (i) the horizontal velocity components are much larger than the vertical ones $u^2,\ v^2 \gg w^2$, (ii) the horizontal length scales are much larger than the vertical ones so that the vertical gradients are much larger than the horizontal ones. The latter feature explains why we assume the horizontal gradients to be negligibly small.

Definitions (65)–(67) allow us to calculate the relative helicity as

$$\sigma = \frac{H}{\sqrt{E\, Z}}. \tag{68}$$

Along with the ratio $|H|/E$, the relative helicity σ serves as a measure to estimate the dominance of kinetic helicity. In the framework of this study, a large ratio of kinetic helicity to kinetic energy and $\sigma \approx 1$ suggest a helicity-dominated regime. The small values of the ratio of kinetic helicity to kinetic energy and $\sigma \approx 0$ represent energy-dominated dynamics.

Both the kinetic energy, the kinetic helicity and the kinetic enstrophy are, concerning the extent of the altitude segments, extensive quantities. Therefore, the mean densities, $\bar{e}$, $\bar{h}$, and $\bar{z}$, for these quantities were calculated for each altitude segment by dividing the respective quantity by the vertical extent of the altitude segment.

As a measure for the magnitude of stratification, the Brunt-Väisälä frequency is calculated pointwise using (4) and subsequently averaged to obtain the Brunt-Väisälä frequency of the altitude segment. The pointwise mass density of the flow is obtained from the vertical profiles of the pressure $p(z)$ and the temperature $T(z)$ contained in the balloon data, assuming the flow to behave as an ideal gas.

The Brunt-Väisälä frequency, along with the vertical gradients $\partial_z u$ and $\partial_z v$ of the horizontal velocity components, enabled us to calculate the Richardson number Ri for each altitude segment, as well. A complete set of flow parameters for each altitude segment is given in Table III.

The kinetic energy spectrum $E(k)$ and the kinetic helicity spectrum $H(k)$ were defined as

$$E(k_z) = \mathcal{F}\{u\}\ \mathcal{F}\{u\}^* + \mathcal{F}\{v\}\ \mathcal{F}\{v\}^*, \tag{69}$$

$$H(k_z) = |-\mathcal{F}\{u\}\ \mathcal{F}\{\partial_z v\}^* + \mathcal{F}\{v\}\ \mathcal{F}\{\partial_z u\}^*|, \tag{70}$$

with $\mathcal{F}$ denoting the Fourier transform operator. The Fourier transforms of the respective functions are obtained using MATLAB's fft function [39]. To reduce the noise in the spectra, all functions were multiplied by a Blackman-Harris window [40] before being Fourier transformed.

B. Results

The spectra for kinetic energy and kinetic helicity in different altitude segments of both datasets are shown in Figs. 3 and 4. Each altitude segment is represented by a k_z axis that starts from the wave number $k_{\min} = 2\pi L_z^{-1}$, where L_z is the vertical extent of the segment. The spectra are confined

TABLE III. The table presents a summary of calculated characteristic values for six predefined altitude segments. It contains estimations for the Brunt-Väisälä frequency N, the Richardson number Ri, as well as integral calculations for the kinetic energy E, kinetic helicity H, and kinetic enstrophy Z_v along with their respective mean densities $\bar{e}$, $\bar{h}$, $\bar{z}_v$ and the relative helicity σ. κ_E and κ_H are obtained from a fit as the exponents of k_z are obtained from spectral fits of kinetic energy $E(k_z)$ and kinetic helicity $H(k_z)$.

	2021			2022		
	[5 km, 8.5 km]	[8.5 km, 13 km]	[13 km, 18 km]	[4 km, 8.5 km]	[8.5 km, 12 km]	[12 km, 15 km]
N [s^{-1}]	0.0381	0.0402	0.0389	0.0361	0.0383	0.0448
Ri	0.17	0.63	1.81	1.35	0.80	0.42
E [m^3 s^{-2}]	11.06×10^5	11.92×10^5	1.17×10^5	4.93×10^5	4.11×10^5	2.84×10^5
$\bar{e}$ [m^2 s^{-2}]	330.3	264.6	23.1	111.2	117.2	95.4
H [m^2 s^{-2}]	212.4	−29.2	207.6	−18.0	29.1	73.0
$\bar{h}$ [m s^{-2}]	0.0630	−0.0070	0.0410	−0.0040	0.0080	0.0250
Z_v [m s^{-2}]	2.2	6.3	6.4	7.6	7.2	8.1
$\bar{z}_v$ [s^{-2}]	6.49×10^{-4}	13.94×10^{-4}	12.65×10^{-4}	17.17×10^{-4}	20.60×10^{-4}	27.26×10^{-4}
$\lvert H\rvert/E$ [m^{-1}]	1.92×10^{-4}	0.25×10^{-4}	17.70×10^{-4}	0.37×10^{-4}	0.71×10^{-4}	2.57×10^{-4}
$\lvert\sigma\rvert$	0.1370	0.0110	0.2390	0.0090	0.0170	0.0480
κ_E	2.0	2.4	3.2	2.6	2.4	2.4
κ_H	1.1	1.2	2.4	1.4	1.2	1.4

within the wave number $k_{\max} = 2\pi l_{\min}^{-1}$, where $l_{\min} = 50$ m that denotes the effective maximum resolution of the data.

The power-law exponents κ_E and κ_H are obtained by fitting the spectrum of kinetic energy and kinetic helicity for each altitude segment. The spectral fits are depicted in Figs. 3 and 4 with orange lines. Each fit is performed in the scale range between $l_{\min} = 50$–75 m and $l_{\max} = 1100$–1300 m. Table III provides a summary of κ_E and κ_H values. Several spectra exhibit a plateau at large scales and increased energy below the resolution scale due to instrumental noise. Trends on the raw data cause spectral leakage on the FFT data that induces the plateau at large scales. The technical distortions on the balloon data, such as pendulum motions and GPS noise, cause the overshoot at small scales. We exclude both spectral effects from performed fits.

For the 2021 data, the stratification increases with altitude, as evidenced by the increase in Ri. The kinetic energy E in the altitude segment between 8.5 km and 13 km is slightly higher than in the segment [5 km, 8.5 km], which is likely to be caused by the difference in altitude coverage, with the former covering 4.5 km and the latter covering 3.5 km. As kinetic energy is a quantity that increases with the size of the segment, it is typically large for wide altitude ranges. Due to the decrease in the absolute value of horizontal velocities, mean kinetic energy density $\bar{e}$ and locally contained kinetic energy E significantly decrease in the upper segment, as seen in Fig. 1. The absolute values of the kinetic helicity $|H|$ and its mean density $\bar{h}$ are the largest for the lowest altitude segment. The relative helicity σ in the altitude segment ranging from 13 km to 18 km is the highest among the 2021 data. This observation correlates with a decrease of $\bar{e}$. Unlike the lowest segment, where a significant decrease of enstrophy induced high σ values, the decrease of σ in the upper segment is dominated by the kinetic energy. The altitudinal behavior of the ratio $|H|/E$ approximately correlates with the behavior of σ in the middle and upper segments. As shown in Table III, an increase in κ_E and κ_H can be observed with altitude for all the observations, indicating that the spectra tend to become steeper with altitude, as can also be seen in Fig. 3.

For the 2022 dataset shown in Table III, the Richardson number decreases with altitude, which is qualitatively different from what we had seen in the 2021 dataset. The decrease in total kinetic energy with height is due to decreasing altitude segment size. However, the mean density $\bar{e}$ remains

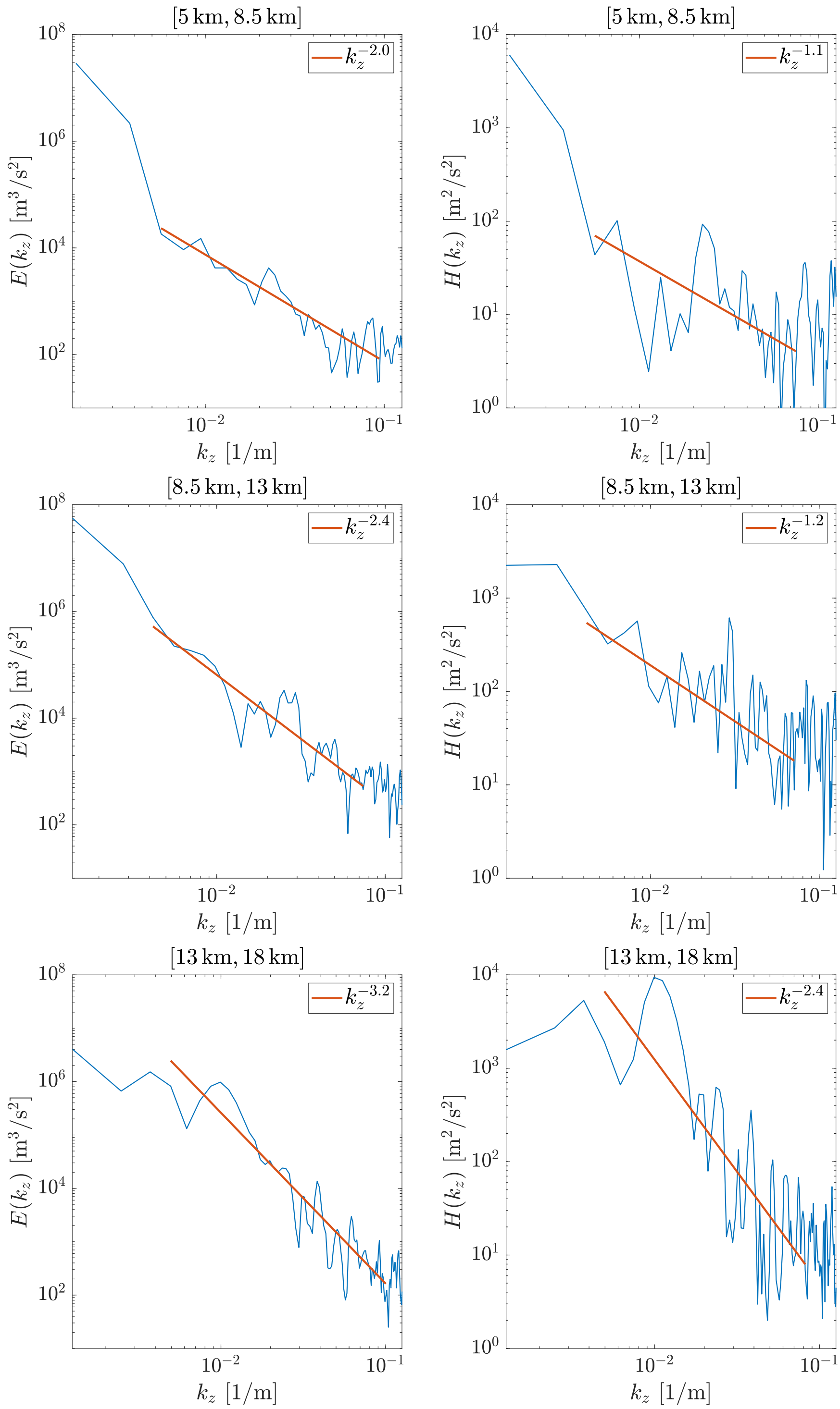

FIG. 3. Kinetic energy (left column) and kinetic helicity (right column) spectra (blue) for the three different altitude segments of the 2021 data along with the fit functions (orange). The data describing the fits is given in Table III. The slopes of the fits for the kinetic energy and the kinetic helicity, respectively, increase throughout the altitude segments so that the spectra become steeper.

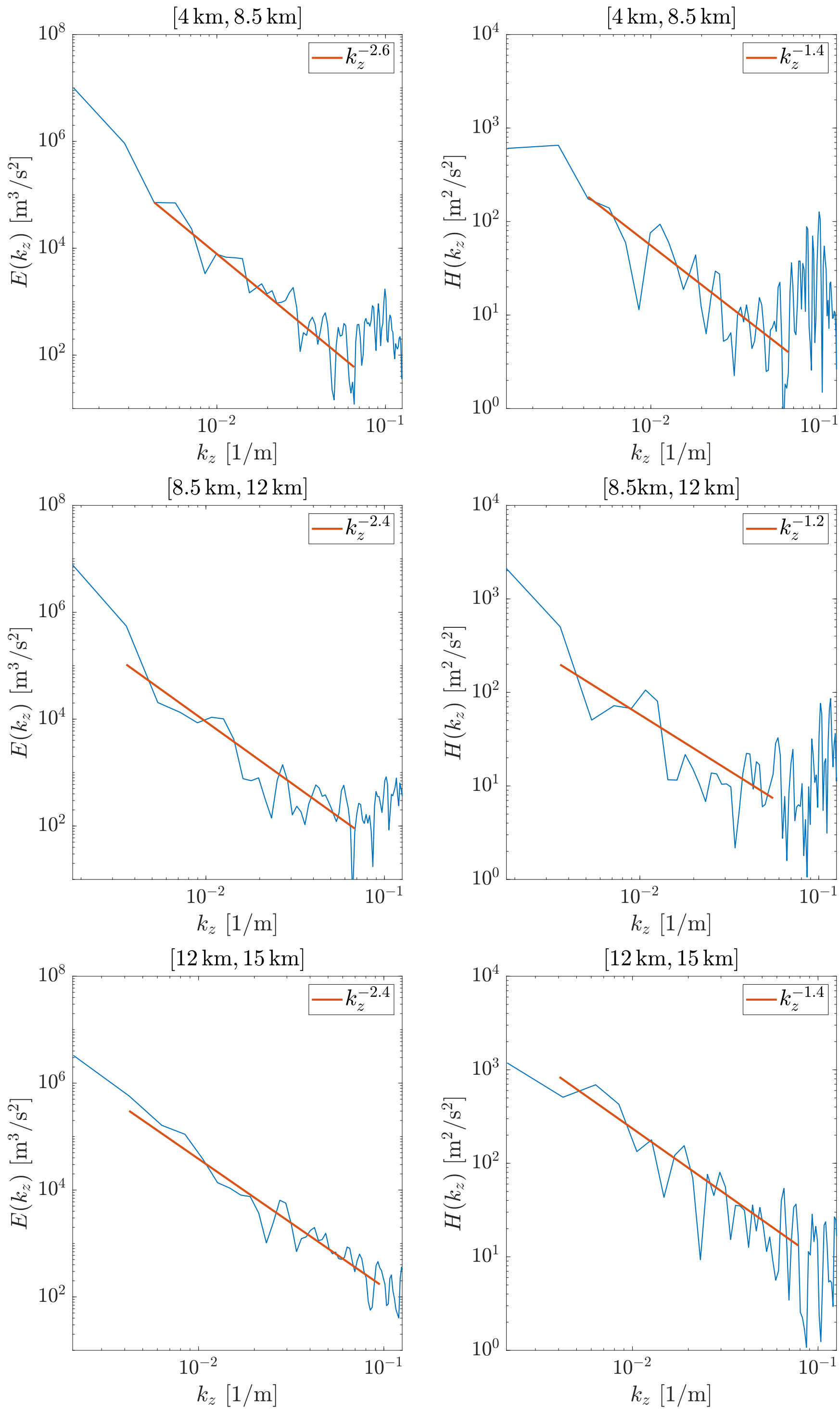

FIG. 4. Kinetic energy (left column) and kinetic helicity (right column) spectra (blue) for the three different altitude segments of the 2022 data along with the fit functions (orange). The data describing the fits is given in Table III. The slopes of the fits for the kinetic energy and the kinetic helicity, respectively, hardly differ throughout the altitude segments.

approximately constant. The kinetic helicity H and its mean density $\bar{h}$ already visibly increase in their absolute values for the altitude segment between 8.5 km and 12 km compared to the lower altitude segment and are of about one order of magnitude higher in the upper segment. The extending role of kinetic helicity is also visible by the relative helicity σ and $|H|/E$ ratio, which increase with the altitude. There is no clear trend for the spectral slopes of kinetic energy and helicity throughout the three altitude segments of the 2022 dataset, as seen in Table III. Finally, it is relevant to note that the fits of κ_E and κ_H values obtained from the 2021 and 2022 datasets have remaining ambiguity caused by the length of the dataset statistics and the fitting ranges.

C. Discussion

Despite these data shortcomings, we can draw general conclusions from these datasets. First, as to the data in Table III, comparing all six segments, a higher Richardson number Ri seems to be related to higher values for κ_E and κ_H. Sorting all six altitude segments by Ri, this tendency is valid for κ_E. For κ_H, there is only a deviation concerning the [12 km, 15 km] altitude segment of the 2022 dataset. This segment has a lower Richardson number than the [8.5 km, 13 km] segment of the 2021 dataset and the [8.5 km, 12 km] segment of the 2022 dataset but a higher value of κ_H.

A growing value of Ri indicates an increasing stratification of the flow. Following the results of Sec. II, it also suggests a change of the eddy distortion time and a higher value of m. The theoretical results from Sec. II support the observation of steepening spectra of kinetic energy and kinetic helicity with increasing stratification and extended distortion time of the flow.

Another relevant observation concerns the role of kinetic helicity. Analysis of all altitude segments reveals that higher values of σ and $|H|/E$ can be the reason for the spectra shallowing. Thus, two main dynamic characteristics affect the cascading properties of the flow. These are stratification, which steepens spectra of kinetic energy and helicity, and helicality, which shallows them. Perhaps the most peculiar effect of the interplay of these different characteristics is obtained in the [13 km, 18 km] segment of the 2021 dataset. Here, the stratification dominates over the significant helical shallowing, and both spectra exhibit distinct stratification dynamic effects.

A slight deviation from the proposed dynamic interplay is observed in the kinetic helicity spectrum of the [12 km, 15 km] altitude segment of the 2022 dataset, which is not explicable based on the compiled quantities. Apart from that, the role of kinetic helicity appears to affect the spectra such that altitude segments with a lower value of σ and weaker influence of kinetic helicity have steeper spectra of kinetic energy and helicity, and segments with larger relative helicity have shallower spectra.

Observing that the change of shape of the spectra would be explicable both based on the effects of stratification and kinetic helicity, the question arises whether or how these effects interact in some way. Indeed, Ref. [14] provides the relation

$$\langle H\rangle_{\perp,z} = \frac{N}{f}\left\langle \theta\frac{\partial w}{\partial z}\right\rangle_{\perp,z}. \tag{71}$$

Here, the volume-averaged kinetic helicity in the approximation based on the scaling of stratified flows on the left-hand side is balanced by the combination of the Brunt-Väisälä frequency N, the Coriolis parameter f, the buoyancy θ and the vertical gradient of the vertical component of the flow velocity on the right-hand side. Therefore, following the statements formulated above, Eq. (71) suggests that the effects of kinetic helicity, stratification, and rotation are coupled. Nevertheless, a quantitative analysis of this relation would go beyond the scope of the discussion of the underlying data of this study and should be the subject of future considerations.

The influence of the density change with altitude on the calculated spectra was analyzed in the present study, as well. In particular, we analyzed spectra of kinetic energy and helicity obtained using the normalized velocity profiles $u(z)\cdot\rho(z)$ and $v(z)\cdot\rho(z)$. An insignificant shallowing of the spectra was observed at the largest scales, while for wave numbers of about $k_z = 10^{-2}$, the density effects were unrecognizable.

The improvements in the balloon measurements are indispensable for our study due to their enhancement in effective wind data resolution by a factor of six compared to a standard radiosonde [37].

IV. CONCLUSION

In this study, we analyzed the role of kinetic helicity in stratified turbulent flows. Based on the idea that the interplay of stratification and kinetic helicity can influence the spectral properties of the flow, it became possible to derive generalized spectral expressions for various energy- and helicity-dominated cases. This study merges and extends the theoretical approaches from Kurien *et al.* [27], concerning the different time scales relevant to the turbulent flow, and Pouquet and Mininni [28], concerning an equivalent consideration for rotating turbulence. As these studies only refer to isotropic or rotational flows, the present study provides new theoretical results for the flows with vertical stratification. Introducing the scaling parameter (m) to quantify the effect of stratification on the distortion of turbulent eddies, we were able to cover various cascading scenarios considering different levels of stratification.

In addition to the influence of stratification, we distinguished cases of either energy- or helicity-dominated regimes for energy-only, helicity-only, and joint cascade scenarios. Based on this theoretical consideration, it was possible to reproduce well-known forms of the spectra and to deduce general statements on how an increasing dominance of either kinetic energy or helicity and different strengths of stratification could influence the spectra of kinetic energy and helicity. The emergence of the Moiseev-Chkhetiani scale ($l_h = \varepsilon_E/\varepsilon_H$) in the dual cascading scenarios for cases with strong stratification ($m \to \infty$) highlights the importance of the coupled consideration for the kinetic energy and helicity spectra. This part of the study concludes that the kinetic helicity domination appears to flatten these spectra compared to the dominance of kinetic energy, and an increasing influence of stratification steepens both helicity and energy spectra.

An analysis of measurement datasets was performed to test the results from Sec. II. Wind data in different atmospheric altitude segments between 4 km and 18 km acquired by balloon measurements were employed to calculate spectra of kinetic energy and helicity and characteristic parameters of the altitude segments. It was possible to make general statements on the impact of stratification on the spectra at various altitude segments and to derive trends that are related to a different influence of these quantities. The primary result of this part of the study is that the observations made in the data analysis follow the theoretical consideration from Sec. II. In particular, the observation that $k_E > k_H$ in all altitude segments suggests that the energy-dominated cascades prevail in the considered datasets. Considering vertical resolution, size of statistics, and other dataset shortcomings, such as the lack of measurements of vertical velocity and its horizontal gradients, we propose that high k_E, k_H values obtained in the [13 km, 18 km] segment of the 2021 dataset are signs of the newly found energy-dominated dual cascade scenario with strong stratification [see Eqs. (45), (46)].

In conclusion, from the theoretical considerations and the results from the analysis of the measurements, kinetic helicity seems to be a quantity that can extend our understanding of stratified turbulence and its spectral properties. The present study proposes a coupled consideration approach (kinetic energy and helicity spectra) to explore the physical properties of stratified turbulent flows.

ACKNOWLEDGMENTS

V.A. acknowledges partial support of his research by the Leibniz Association (Germany) via the SAW project FORMOSA. V.A. and N.D. acknowledge partial support of their research by the Deutsche Forschungsgemeinschaft (DFG, German Research Foundation) under Grant No. 520013270 (2023). The authors thank Fabio Feraco for a critical reading of the manuscript. The authors express their gratitude to the two anonymous referees whose insightful comments greatly improved this work.

[1] L. F. Richardson, Weather prediction by numerical process, Q. J. R. Meteorolog. Soc. **48**, 282 (1922).
[2] A. N. Kolmogorov, V. Levin, J. C. R. Hunt, O. M. Phillips, and D. Williams, The local structure of turbulence in incompressible viscous fluid for very large Reynolds numbers, Proc. R. Soc. Lond. A **434**, 9 (1991).
[3] G. D. Nastrom and K. S. Gage, A climatology of atmospheric wavenumber spectra of wind and temperature observed by commercial aircraft, J. Atmos. Sci. **42**, 950 (1985).
[4] J.-R. Alisse and C. Sidi, Experimental probability density functions of small-scale fluctuations in the stably stratified atmosphere, J. Fluid Mech. **402**, 137 (2000).
[5] O. M. Phillips, *The Dynamics of the Upper Ocean*, 2nd ed. (Cambridge University Press, New York and London, 1977)
[6] E. Lindborg, The energy cascade in a strongly stratified fluid, J. Fluid Mech. **550**, 207 (2006).
[7] G. Brethouwer, P. Billant, E. Lindborg, and J.-M. Chomaz, Scaling analysis and simulation of strongly stratified turbulent flows, J. Fluid Mech. **585**, 343 (2007).
[8] A. Maffioli, Vertical spectra of stratified turbulence at large horizontal scales, Phys. Rev. Fluids **2**, 104802 (2017).
[9] J. J. Moreau, Constantes d'un îlot tourbillonnaire en fluide parfait barotrope, Comptes rendus hebdomadaires des séances de l'Académie des sciences **252**, 2810 (1961).
[10] H. K. Moffatt, The degree of knottedness of tangled vortex lines, J. Fluid Mech. **35**, 117 (1969).
[11] H. K. Moffatt and A. Tsinober, Helicity in laminar and turbulent flow, Annu. Rev. Fluid Mech. **24**, 281 (1992).
[12] A. Brissaud, U. Frisch, J. Leorat, M. Lesieur, and A. Mazure, Helicity cascades in fully developed isotropic turbulence, Phys. Fluids **16**, 1366 (1973).
[13] E. Deusebio and E. Lindborg, Helicity in the ekman boundary layer, J. Fluid Mech. **755**, 654 (2014).
[14] R. Marino, P. D. Mininni, D. Rosenberg, and A. Pouquet, Emergence of helicity in rotating stratified turbulence, Phys. Rev. E **87**, 033016 (2013).
[15] C. Rorai, P. D. Mininni, and A. Pouquet, Stably stratified turbulence in the presence of large-scale forcing, Phys. Rev. E **92**, 013003 (2015).
[16] C. Rorai, D. Rosenberg, A. Pouquet, and P. D. Mininni, Helicity dynamics in stratified turbulence in the absence of forcing, Phys. Rev. E **87**, 063007 (2013).
[17] D. Rosenberg, A. Pouquet, R. Marino, and P. D. Mininni, Evidence for bolgiano-obukhov scaling in rotating stratified turbulence using high-resolution direct numerical simulations, Phys. Fluids **27**, 055105 (2015).
[18] J. Baerenzung, D. Rosenberg, P. D. Mininni, and A. Pouquet, Helical turbulence prevails over inertial waves in forced rotating flows at high Reynolds and low Rossby numbers, J. Atmos. Sci. **68**, 2757 (2011).
[19] G. Levina, Parameterization of helical turbulence in numerical models of intense atmospheric vortices, in *Doklady earth sciences* (Springer, Berlin, 2006), Vol. 411(2), p. 1417.
[20] R. Hide, Superhelicity, helicity and potential vorticity, Geophys. Astrophys. Fluid Dyn. **48**, 69 (1989).
[21] M. V. Kurgansky, On the relation between helicity and potential vorticity in an compressible rotating fluid, Izvestiia Akademii nauk SSSR. Fizika Atmosfery i Okeana **25**, 1326 (1989).
[22] M. V. Kurgansky, *Adiabatic Invariants in Large-Scale Atmospheric Dynamics* (Taylor & Francis, London and New York, 2002).
[23] O. G. Chkhetiani, On the helical structure of the Ekman boundary layer, Izvestiia-Russian Academy of Sciences Atmospheric and Oceanic Physics C/C of Izvestiia-Rossiiskaia Akademiia Nauk Fizika Atmosfery i Okeana **37**, 569 (2001).
[24] V. M. Ponomarev and O. G. Chkhetiani, Semiempirical model of the atmospheric boundary layer with parametrization of turbulent helicity effect, Izvestiia-Russian Academy of Sciences Atmospheric and Oceanic Physics C/C of Izvestiia-Rossiiskaia Akademiia Nauk Fizika Atmosfery i Okeana **41**, 418 (2005).
[25] O. G. Chkhetiani, M. V. Kurgansky, and N. V. Vazaeva, Turbulent helicity in the atmospheric boundary layer, Boundary-Layer Meteorology **168**, 361 (2018).
[26] N. Vazaeva, O. Chkhetiani, M. Kurgansky, and M. Kallistratova, Helicity and turbulence in the atmospheric boundary layer, Izvestiya, Atmos. Ocean. Phys. **57**, 29 (2021).

[27] S. Kurien, M. A. Taylor, and T. Matsumoto, Cascade time scales for energy and helicity in homogeneous isotropic turbulence, Phys. Rev. E **69**, 066313 (2004).

[28] A. Pouquet and P. D. Mininni, The interplay between helicity and rotation in turbulence: implications for scaling laws and small-scale dynamics, Philos. Trans. R. Soc. A **368**, 1635 (2010).

[29] R. H. Kraichnan, Inertial-range transfer in two-and three-dimensional turbulence, J. Fluid Mech. **47**, 525 (1971).

[30] V. E. Zakharov, V. S. L'vov, and G. Falkovich, *Kolmogorov Spectra of Turbulence 1. Wave Turbulence* (Springer, Berlin, 1992).

[31] S. Nazarenko, *Wave Turbulence* (Springer, Berlin, 2011).

[32] J. Weinstock, On the theory of turbulence in the buoyancy subrange of stably stratified flows, J. Atmos. Sci. **35**, 634 (1978).

[33] E. M. Dewan and R. E. Good, Saturation and the "universal" spectrum for vertical profiles of horizontal scalar winds in the atmosphere, J. Geophys. Res.: Atmos. **91**, 2742 (1986).

[34] V. Avsarkisov, On the buoyancy subrange in stratified turbulence, Atmos. **11**, 659 (2020).

[35] S. S. Moiseev and O. Chkhetiani, Helical scaling in turbulence, J. Exp. Theor. Phys. **83**, 192 (1996).

[36] O. Chkhetiani, On the third moments in helical turbulence, J. Exp. Theor. Phys. Lett. **63**, 808 (1996).

[37] J. Faber, M. Gerding, and T. Köpnick, Acquiring high-resolution wind measurements by modifying radiosonde sounding procedures, Atmos. Meas. Tech. **16**, 4183 (2023).

[38] V. Avsarkisov, E. Becker, and T. Renkwitz, Turbulent parameters in the middle atmosphere: Theoretical estimates deduced from a gravity wave–resolving general circulation model, J. Atmos. Sci. **79**, 933 (2022).

[39] M. Frigo and S. G. Johnson, FFTW: An adaptive software architecture for the FFT, in *Proceedings of the 1998 IEEE Intl. Conf. Acoustics Speech and Signal Processing* (IEEE, New York, 1998), Vol. 3, pp. 1381–1384.

[40] F. Harris, On the use of windows for harmonic analysis with the discrete fourier transform, Proc. IEEE **66**, 51 (1978).